https://doi.org/10.3311/PPee.44636

Periodica Polytechnica Electrical Engineering and Computer Science

Research on Fault Recovery of Electricity-gas Coupled Systems Based on Risk Early Warning

Xiaojuan Lu[1], Qixuan Liu[1*], Duojin Fan[1], Zhiyong Zhang[1]

[1] School of Automation and Electrical Engineering, Lanzhou Jiaotong University, 88 Anning West Road, 730070 Lanzhou, China
* Corresponding author, e-mail: 1272025718@qq.com

Received: 09 May 2026, Accepted: 06 August 2026, Published online: 22 September 2026

Abstract

To address the large-scale blackout problem caused by cascading faults in the electricity-gas coupled system triggered by extreme weather, this study proposes a long-term phased restoration plan for outage loads through the coordinated operation of soft open points (SOPs) and energy storage devices. Firstly, considering the power flow regulation characteristics of SOPs, the power supply capacity of energy storage, and the safety constraints of the gas network, an optimization model for fault recovery is established, with the objectives of maximizing power supply guarantee rate, minimizing network loss, and ensuring the safe and stable operation of the gas network. Secondly, drawing on the idea of risk prevention and control, a risk assessment model is constructed from two dimensions: equipment operation reliability and fault power loss consequences, and the grey relational improved TOPSIS method is adopted to complete the priority ranking of critical loads. Finally, a phased fault reconfiguration and maintenance strategy coordinated by SOPs and energy storage is formulated, and multi-period rolling optimization is carried out to realize continuous power supply during the maintenance period. Simulation results show that the proposed method can effectively block the cross-domain cascading fault propagation path from the power grid to the gas network, providing technical support for the emergency disposal of large-scale blackout accidents in similar coupled systems

Keywords

electricity-gas coupled system, risk assessment, soft open point, fault recovery

1 Introduction

Against the backdrop of the global energy structure transitioning toward cleanliness and low carbonization, the electricity-gas coupled system, leveraging its technical advantage of multi-energy complementarity, has become the core form of the new power system. However, its deep interconnection characteristics also expose the system to more complex cascading failure risks [1]. For instance, during the "8·9" blackout in the UK in 2019, a lightning strike caused a line short circuit, resulting in a 1.3 GW power loss in the power grid. This surge in power demand further led to a collapse in gas network pressure due to the skyrocketing gas consumption of gas-fired units, affecting 1 million people [2–3]. Similarly, the 2021 Texas blackout in the United States was exacerbated by ice blockages in natural gas pipelines, which caused the shutdown of some gas-fired units and further worsened the disaster [4]. Such incidents not only highlight the cascading effect and destructive consequences of faults in the electricity-gas coupled system but also reveal common issues such as the lack of cross-system collaborative control and inadequate emergency response plans, sounding the alarm for the development of power grid.

Notably, the "dual-high and dual-low" characteristics of the UK power grid—characterized by high penetration of renewable energy, high integration of power electronic devices, low inertia, and low anti-disturbance capability—are gradually becoming the new normal in the development of China's distribution networks [5–6]. Coupled with the in-depth integration of electrical and gas networks, a single fault in traditional distribution networks can easily evolve into a systemic blackout accident through the coupling chain [7–8]. Currently, Jia and Huang [9] show optimal scheduling models based on SOPs, which effectively improve the reliability and economy of the system. Nacef et al. show [10] have developed a fault-tolerant control strategy for seven-level cascaded inverters in photovoltaic systems, enhancing the operational performance and stability

Cite this article as: Lu, X., Liu, Q., Fan, D., Zhang, Z. "Research on Fault Recovery of Electricity-gas Coupled Systems Based on Risk Early Warning", Periodica Polytechnica Electrical Engineering and Computer Science, 2026. https://doi.org/10.3311/PPee.44636

of renewable energy systems. Al-Dwa et al. show [11] have developed a transformation scheme for grid-connected four-leg voltage source inverters (GC-FLVSIs), achieving precise current control and high-quality smooth grid integration performance. Additionally, Kang and Hu et al. [12–13] have developed fault reconfiguration models based on SOPs, enhancing the load recovery capability of distribution networks. He et al. [14] has linked fault recovery with reinforcement learning, improving the adaptive capability of distribution networks. Peng et al. [15] have developed a multi-stage game-theoretic fault restoration method for electricity-gas integrated energy systems under the coordination of network reconfiguration and rush repair, but this work insufficiently accounts for system safety boundary constraints under extreme operating conditions, implying potential risks of secondary faults induced by power and gas flow violations. Zhang et al. [16] have proposed a two-stage intra-disaster and post-disaster coordinated optimization strategy integrating fault restoration and maintenance scheduling for resilience enhancement of electricity-gas integrated energy systems, but the system safety margin under extreme cascading fault scenarios still has room for improvement. With network reconfiguration mainly relying on discrete actions of traditional switches, the restoration granularity and operational safety can be further promoted by introducing flexible regulation devices such as SOPs. Zhang [17] has established a comprehensive reliability evaluation framework incorporating the temporal characteristics of distributed generators, various coupling devices, and natural gas network operation laws, addressing the limitation that traditional assessment methods for independent electricity-gas systems fail to capture bidirectional multi-energy coupling operational features. Ye et al. [18] have developed a cascading failure risk assessment model for the integrated power system of unmanned platforms, conducting risk evaluation on a typical medium-voltage DC (MVDC) integrated power system. Zhang et al. [19] quantified the extreme risk of gas network faults and established a cascading fault model for the electrical-gas coupled system considering the impact of the extreme risk of natural gas networks. Wang et al. [20] established an electrical-thermal coupled system model for the coordinated reconfiguration of distribution networks and heating networks, effectively improving the reliability of the coupled system. Yang and Yan et al. [21–22] reviewed the typical forms, coupling mechanisms, and safety assessment methods of electrical-gas coupled systems, providing perspectives for the future development of safety assessment for electrical-gas coupled systems. Bahlouli et al. [23] established a bi-level optimization model for the configuration of user-side emergency power sources that meets the resilience guarantee level of a robust local power grid against the background of the loss of main grid power support, thereby obtaining the minimum-cost emergency power source configuration decision result that enables the distribution network to meet the resilience requirements. Although existing studies have carried out in-depth research on core issues related to the safe and stable operation of electrical-gas integrated energy systems, such as fault mechanisms, propagation paths, and defense strategies, revealed the evolution laws of single faults, and proposed various response methods including network reconfiguration, flexible regulation, and emergency scheduling, providing important theoretical and technical support for system safety defense [24], the existing achievements generally remain at the level of single-system fault handling or coordinated control under loose coupling, and have not truly solved the cross-domain cascading failure problem caused by the electrical-gas strong coupling mechanism itself:

1. Most studies decouple the analysis of power grid fault recovery from gas grid safety constraints, failing to consider the bidirectional energy transfer amplification effect of coupled equipment such as gas turbines and compressors under faults, which cannot block the closed-loop cascading path of "power grid fault → gas grid pressure fluctuation → sudden change in gas turbine output → further power grid instability";
2. Existing methods lack a dynamic response mechanism for the development stage of cascading faults, making it difficult to achieve adaptive switching between maximum load recovery and gas grid safety guarantee. Once a fault is triggered across domains, it is prone to cause systemic collapse;
3. Emergency plans for hidden risks are insufficient, and the emergency response capability for severe faults of N-1 and above is weak.

To address the aforementioned dilemmas, there is an urgent need to construct a proactive reconfiguration prevention strategy based on risk early warning, realizing the transformation from post-event recovery to pre-event prevention and control. Based on this, this paper draws on the experience of major blackout accidents abroad to carry out research on cascading fault defense strategies for electrical-gas coupled systems. Firstly, a GT-DFR cascading fault recovery model with gas turbines as key coupling points is established, integrating the millisecond-level power control characteristics of SOPs and the long-term power supply capacity of energy storage, and the model is efficiently solved by the second-order cone relaxation method; secondly, a full-dimensional risk assessment system covering equipment operating status, environmental disturbance factors, and fault power outage consequences is constructed, and the grey correlation-improved TOPSIS method is adopted to realize the risk ranking of critical loads; finally, a reconfiguration prevention strategy is proposed, which, combined with the construction of a contingency set, achieves continuous and reliable power supply for critical loads during maintenance periods under extreme weather, optimizes system power distribution, and greatly improves the local consumption rate and energy utilization efficiency of distributed renewable energy.

2 Cascading fault and recovery model of the electrical-gas coupled system

As shown in Fig. 1, GT-DFR is a model designed for distribution network fault scenarios in electrical-gas integrated energy systems. Taking gas-electric conversion equipment such as gas turbines as key coupling points, it establishes a unified mathematical model. On the premise of ensuring the safe and reliable reconfiguration of the power grid and the physical operation constraints of the gas grid, it coordinately optimizes the switching operations of the power grid, unit scheduling, and resource allocation of the gas grid, and finally achieves a balance between the optimal overall recovery effect and economic optimization of the system after faults. Among them, the energy storage systems carried by the photovoltaic power stations at Nodes 7 and 13 can participate in regulation.

2.1 Objective function

According to the load demand of distribution network nodes, this paper gives priority to load recovery and then considers network loss when performing network reconfiguration. The objective function is as Eqs. (1–3):

$$F_1 = \min \begin{bmatrix} \omega_1 \sum_{i\in\Omega_{P,1}} P_{i,t}^L\left(1-\alpha_i\right)+ \\ \omega_2 \sum_{i\in\Omega_{P,2}} P_{i,t}^L\left(1-\alpha_i\right)+ \\ \omega_3 \sum_{i\in\Omega_{P,3}} P_{i,t}^L\left(1-\alpha_i\right) \end{bmatrix}, \tag{1}$$

$$F_2 = \min I^2 R\,, \tag{2}$$

$$F = F_1 + \mu F_2\,. \tag{3}$$

Where: ω_1, ω_2 and ω_3 are the weight coefficients of primary, secondary, and tertiary loads, respectively; $P_{i,t}^L$ represents the original load power at node ; α_i represents the node load recovery coefficient; $\Omega_{P,v}$ denotes the set of distribution network nodes; μ is a very small number, which

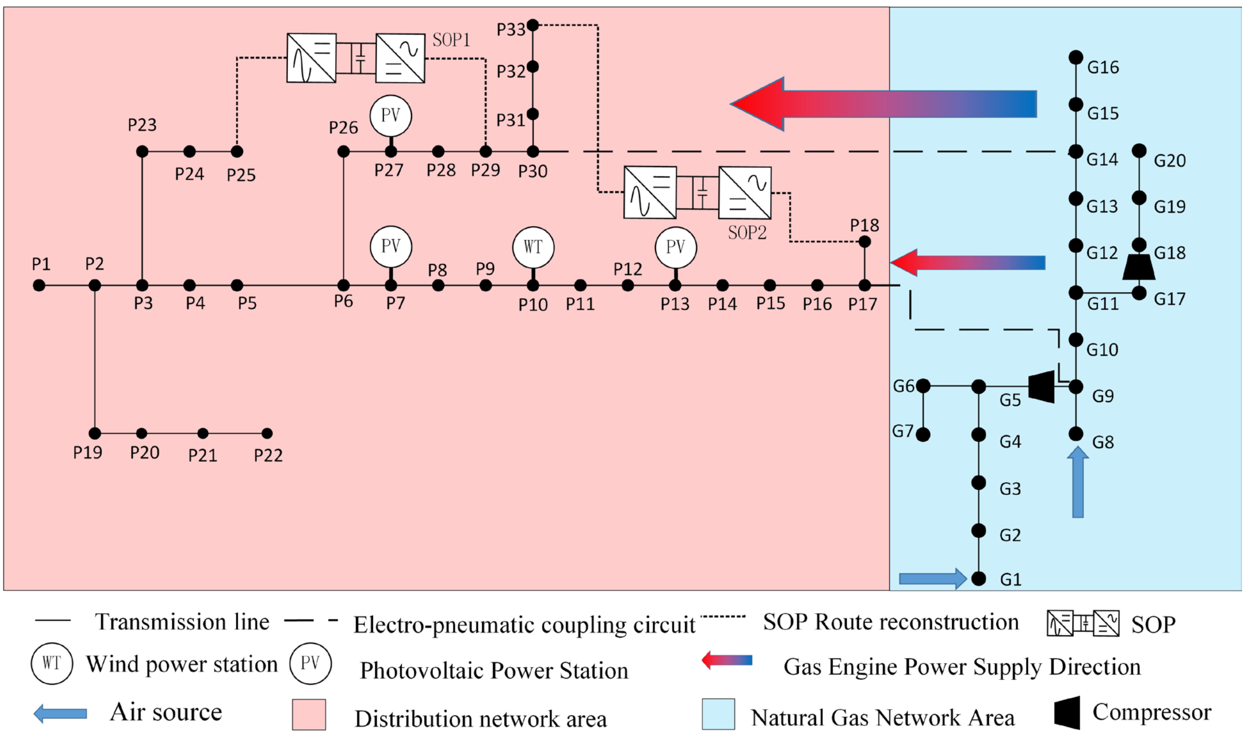

Fig. 1 GT-DFR model

reduces the impact of distribution network loss on the results, thereby highlighting the load recovery capability.

Table 1 summarizes the importance classification of loads at each network node. First class loads hold the highest priority, defined as loads whose supply outage will cause personal casualties, catastrophic equipment damage, substantial economic losses, or severe impairment to national security and core urban functionality. Second class loads rank second in supply priority. Their power interruption will incur considerable economic losses, disrupt the normal production and operation of key consumers, or trigger local disorder in urban public order. Third class loads impose no special reliability requirements, as their supply interruption exerts negligible impacts on industrial production and daily life [25].

The natural gas network takes the minimum gas purchase cost as the optimization objective:

$$F_3 = \min \sum\nolimits_{m\in\Omega_G} D_G W_{m,t}^Y . \tag{4}$$

Where: D_G is the gas purchase cost; $W_{m,t}^Y$ is the gas volume that node m of the natural gas network needs to purchase from the upper-level system at time t; Ω_G denotes the set of gas source nodes, and G_1 and G_8 are the gas source nodes in this paper.

2.2 Model establishment

1) SOP Constraints

The SOP adopting back-to-back voltage source converters used in this paper adjusts its control scheme through different operations. There are two types of SOP control schemes: the first is the UdcQ-PQ scheme, which is suitable for precise power control in grid-connected environments, directly responds to scheduling requirements, and improves energy efficiency and flexibility; when a fault occurs in the distribution network of this paper, the second UdcQ-Uacf scheme is adopted, which is suitable for scenarios that need to independently maintain grid stability. It indirectly manages power by regulating voltage and frequency, thereby enhancing system robustness [26].

Table 1 Load level and distribution

node set	Load class	Nodes	Weighting coefficient
$\Omega_{P,1}$	First class load	2, 7, 13	10
$\Omega_{P,2}$	Second class load	8, 15, 21, 27	5
$\Omega_{P,3}$	Third class load	3–6, 9–12, 14, 16–20, 22–26, 28–33	1

As shown in Fig. 2, when one side of the SOP is connected to the main grid or a DG with self-starting or energy storage capability, the UdcQ control mode is adopted. The other side adopts the Uacf control mode because it is disconnected from the main grid and has no DG with self-starting capability. The constraints of the SOP are as Eqs. (5–10):

$$P_{s,i,t}^{SOP} + P_{s,j,t}^{SOP} + P_{s,i,t}^{SOP,L} + P_{s,j,t}^{SOP,L} = 0 , \tag{5}$$

$$P_{s,i,t}^{SOP,L} = A_{s,i}^{SOP} \left\| P_{s,i,t}^{SOP} Q_{s,i,t}^{SOP} \right\|_2 , \tag{6}$$

$$P_{s,j,t}^{SOP,L} = A_{s,j}^{SOP} \left\| P_{s,j,t}^{SOP} Q_{s,j,t}^{SOP} \right\|_2 , \tag{7}$$

$$\left\| P_{s,i,t}^{SOP} Q_{s,i,t}^{SOP} \right\|_2 \le S_{s,i}^{SOP} , \tag{8}$$

$$\left\| P_{s,j,t}^{SOP} Q_{s,j,t}^{SOP} \right\|_2 \le S_{s,j}^{SOP} , \tag{9}$$

$$U_{s,i,t}^{SOP} \ge U_0 . \tag{10}$$

Where: $P_{s,i,t}^{SOP}$ and $P_{s,i,t}^{SOP,L}$ respectively represent the active power and active power loss of the s-th SOP at node i and time t; $Q_{s,i,t}^{SOP}$ denotes the reactive power of the s-th *SOP* at node i and time t; $A_{s,i}^{SOP}$ is the power loss coefficient of the s-th *SOP* at node i; $S_{s,i}^{SOP}$ is the capacity of the s-th *SOP* at node i.

2) Distribution System Constraints

The distribution network is in a static state, the constraints are as Eqs. (11–14):

$$\sum\nolimits_{j\in\Omega_{p,\mathrm{in}}(i)} \left(P_{ij,t} - r_{ij} I_{ij,t}^2 \right) + P_{S,i,t} + P_{W,i,t} + P_{s,i,t}^{SOP} - \alpha_i P_{i,t}^L = \sum\nolimits_{k\in\Omega_{p,\mathrm{out}}(i)} P_{ik,t} \tag{11}$$

$$\sum\nolimits_{j\in\Omega_{p,\mathrm{in}}(i)} \left(Q_{ij,t} - x_{ij} I_{ij,t}^2 \right) + Q_{s,i,t}^{SOP} - Q_{i,t}^L = \sum\nolimits_{k\in\Omega_{p,\mathrm{out}}(i)} Q_{ik,t} \tag{12}$$

$$U_{i,t}^2 - U_{j,t}^2 - 2\left(r_{ij} P_{ij,t} + x_{ij} Q_{ij,t} \right) + \left(r_{ij}^2 + x_{ij}^2 \right) I_{ij,t}^2 = 0 \tag{13}$$

$$I_{ij,t}^2 U_{i,t}^2 = P_{ij,t}^2 + Q_{ij,t}^2 \tag{14}$$

Where: $P_{ij,t}$ and $Q_{ij,t}$ are the active power and reactive power flowing into node i at time t, respectively; $P_{ik,t}$

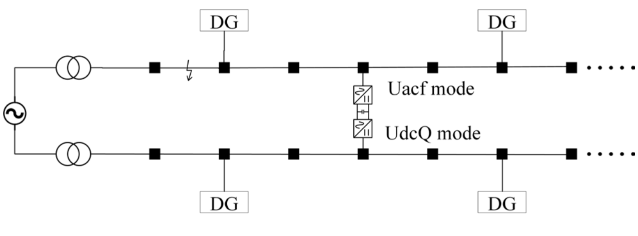

Fig. 2 Post-fault control mode of SOP

and $Q_{ij,t}$ are the active power and reactive power flowing through the *ik* branch at time *t*, respectively; $Q_{i,t}^{L}$ represents the reactive load power at node *i* at time *t*; r_{ij} and x_{ij} represent the resistance and reactance of the upper branch of node *i*, respectively; $P_{S,i,t}$ and $P_{W,i,t}$ represent the power generation power of photovoltaic and wind energy at node *i* at time *t*, respectively; $U_{i,t}^{2}$ and $U_{j,t}^{2}$ represent the amplitude of the voltage at node *i* and node *j*, respectively; $\Omega_{p,\mathrm{in}(i)}$ and $\Omega_{p,\mathrm{out}(i)}$ represent the set of incoming and outgoing distribution network to node *i*, respectively.

3) Gas Turbine Model

In this paper, the gas turbine is regarded as a power source in the distribution network and a load in the natural gas network. Its energy conversion model as a coupling component is as Eqs. (15–16):

$$P_{i,t}^{GT} = \eta_{GT} W_{m,t}^{GT} \tag{15}$$

$$P_{GT,\min} \le P_{GT,t} \le P_{GT,\max} \tag{16}$$

Where: η_{GT} is the energy conversion efficiency of the gas turbine; $W_{m,t}^{GT}$ is the gas input volume of the gas turbine at time *t*; $P_{GT,\min}$ and $P_{GT,\max}$ are the maximum and minimum values of the gas turbine output, respectively.

4) Gas Turbine Ramping Constraints:

$$-\delta_{GT,i}^{u} \Delta t \le P_{GT,i,t} - P_{GT,i,t-1} \le \delta_{GT,i}^{u} \Delta t \tag{17}$$

$$-\delta_{GT,i}^{d} \Delta t \le P_{GT,i,t} - P_{GT,i,t-1} \le \delta_{GT,i}^{d} \Delta t \tag{18}$$

Where: $\delta_{GT,i}^{u}$ and $\delta_{GT,i}^{d}$ represent the upward ramping rate and downward ramping rate of the gas turbine, respectively; *Δt* is the time interval.

5) Gas Distribution Network Model:

In this paper, the gas distribution network is composed of natural gas sources, gas transmission pipelines, gas-consuming compressors, and natural gas loads. Its constraints are as Eqs. (19–23):

$$W_{m,\min}^{Y} \le W_{m,t}^{Y} \le W_{m,\max}^{Y} \tag{19}$$

$$G_m \ge G_n \tag{20}$$

$$G_n^{com} \le \theta G_m^{com} \tag{21}$$

$$G_{m,\min} \le G_{m,t} \le G_{m,\max} \tag{22}$$

$$\begin{aligned}&\sum\nolimits_{m\in\Omega_Y} W_m^{Y} - \sum W_{mn} - \gamma \sum\nolimits_{m\in\Omega_{com}} W_m^{com} - \\ &\sum\nolimits_{m\in\Omega_{GT}} W_m^{GT} = \sum\nolimits_{m\in\Omega_G} W^{L}\end{aligned} \tag{23}$$

Where: $W_{m,t}^{Y}$ represents the gas source output at node *m* at time *t*; G_m represents the gas pressure at node *m* of the natural gas network; G_m^{com} represents the gas pressure at node *m* of the compressor; *γ* represents the gas consumption coefficient of the gas consumed by the compressor; W_m^{com} represents the gas volume consumed by the compressor; *θ* is the compression factor of the compressor; W^L represents the gas volume consumed by the gas load.

The natural gas has very low loss during transportation, but it has characteristics similar to the voltage loss of the power system. Therefore, the Weymouth equation is adopted for the approximate treatment of the gas network in the steady state:

$$W_{mn,t} = S_{mn} C_{mn} \sqrt{\left| G_{m,t}^{2} - G_{n,t}^{2} \right|}\ , \tag{24}$$

$$S_{mn} = \begin{cases} 1 & G_{m,t} > G_{n,t} \\ -1 & G_{m,t} \le G_{n,t} \end{cases}, \tag{25}$$

$$W_{mn,\min} \le W_{mn,t} \le W_{mn,\max}\ . \tag{26}$$

Where: C_{mn} is the pipeline equation parameter, which is related to the physical properties of the pipeline itself such as temperature, length, diameter, and friction; S_{mn} is the gas direction parameter.

2.3 Second-order cone transformation of the model

The above model is a complex mixed-integer nonlinear model, which has low solution efficiency and is difficult to obtain the optimal solution. This paper uses variable substitution and second-order cone relaxation methods to linearize and convexify the model. This method has been introduced and verified in References [27–29], so it will not be elaborated in this paper.

$$\frac{P_{ij,t}^{2} + Q_{ij,t}^{2}}{u_{i,t}} \le i_{ij,t} \tag{27}$$

The above formula is transformed into the second-order cone form as Eq. (28):

$$\left\| \begin{bmatrix} 2P_{ij,t} & 2Q_{ij,t} & i_{ij,t} - v_{i,t} \end{bmatrix}^{T} \right\|_2 \le i_{ij,t} + v_{i,t}\ . \tag{28}$$

Where: $i_{ij,t}$ will be used for replacement; $v_{i,t}$ will be used for replacement.

The pipeline flow equation is transformed into the second-order cone form as Eq. (29):

$$\left\| \begin{matrix} W_{mn,t} \\ C_{mn} G_{m,t} \end{matrix} \right\| \le C_{mn} G_{n,t}\ . \tag{29}$$

The steady-state natural gas network model employed in this work neglects line pack effects. This simplification yields conservative estimates of node pressure margins and the gas supply assurance capacity of gas-fired units, thereby avoiding overestimation of system restoration performance. Furthermore, pressure propagation delays and transient fluctuations only arise during short-term operating condition transitions. Given the hourly time scale of the phased restoration mechanism, these transient phenomena can be fully damped, and thus will neither shift the steady-state operating points of the system nor alter the core conclusions of the optimization scheme [28].

To quantitatively compare the resilience enhancement effects of different strategies, a criterion for natural gas pressure safety margin is established as Eq. (30):

$$M_i = \frac{G_{m,\max} - G_m}{G_{m,\max}} , \tag{30}$$

where M_i denotes the natural gas pressure safety margin.

The model proposed in this paper incorporates a three-tier operational margin guarantee mechanism from the perspectives of constraint configuration, flexible resource reservation and decision-making mechanism, to enhance the scheme's adaptability to source-load fluctuations and operating condition deviations. Reasonable margin coefficients are introduced into security constraints including line current-carrying capacity, node voltage and gas network node pressure, avoiding solutions that lie tightly at operational limits. Meanwhile, a proportion of regulation reserve is retained for the rated converter capacity of SOPs and the available charge-discharge power of energy storage systems, leveraging flexible regulation capability to mitigate the impact of source-load fluctuations. Furthermore, the phased maintenance and restoration scheme supports rolling adjustment and can dynamically revise network reconfiguration strategies according to real-time operating states, collectively ensuring the operational robustness of the overall scheme.

3 Distribution network load risk assessment model

The distribution network has a complex structure and numerous power distribution equipment. If risk prevention and control work is carried out for each power distribution equipment one by one, the scale of the anticipated accident set will expand sharply. Therefore, it is necessary to scientifically set up a risk assessment index system to quantitatively rank various potential risk scenarios, and give priority to implementing precise prevention and control for the top *N* high-risk scenarios, so as to ensure the timeliness and efficiency of fault response while guaranteeing the prevention and control effect. Table 2 lists the names and definitions of special symbols used in this subsection.

This study establishes a contingency accident set to conduct risk assessment on some high-risk equipment or lines, and the model is as Eq. (31):

$$S_z = S_p \times S'_h . \tag{31}$$

Where: S_z is the value of the equipment risk assessment index, S_p is the value of the equipment reliability index; S'_h is the value represented by the consequences of load failure and power outage.

3.1 Equipment reliability indicators

Equipment reliability indicators focus on the probability of equipment failure and the impact of external disturbances, mainly including two types of sub-indicators:

1) Equipment Failure Rate

The aging and failure behavior of distribution network equipment presents significant time-dependent characteristics. Its failure probability can usually be described by exponential distribution, normal distribution or Weibull distribution. Among them, the Weibull distribution can more

Table 2 Nomenclature of selected special symbols

Symbol	Notation	Symbol	Notation
S_z	Equipment risk assessment indicator	S_{loss}	Load power interruption magnitude
S_p	Equipment reliability indicator	S_m	Economic loss of one-hour load outage during fault events
S'_h	Consequence of load outage due to faults	$X_{sq,ij}$	Judgment matrix
S_l	Fault occurrence probability	$e_{sq,j}$	Information entropy of the *j*-th indicator
$\lambda^F_{js,t}$	Fault occurrence rate under extreme rainstorm conditions	λ_j'	Entropy weight of the *j*-th indicator
$P^F_{js}(\Delta t)$	Fault probability within under extreme rainstorm conditions	λ_j''	AHP weight of the *j*-th indicator
$S(U_{\text{LEVEL}})$	Voltage violation risk per unit time	λ_j	Coupled weight of the *j*-th indicator
$S_{h,ij}$	Grey relational matrix	ρ	Resolution coefficient
s^+_{lx0}	Positive ideal target solution	s^-_{lx0}	Negative ideal target solution
$d^+_{lx,i}$	Positive ideal target solution	$d_{lx,i}{}^-$	Distance to the negative ideal target solution
$D_{lx,i}$	Relative closeness degree	v^+_0	Optimal ideal target solution
$\mathit{\Delta}_{ij,t}$	Relaxation error of the distribution network	$\mathit{\Delta}_{mn,t}$	Relaxation error of the natural gas network

accurately describe the complete life cycle law of equipment from early failure, random failure to wear-out failure. Therefore, this study selects this distribution to establish a correlation model of failure probability changing with operating time to evaluate the failure probability within a specific period, which is defined as Eq. (32):

$$S_l = 1 - e^{-\left(\frac{t}{\eta_l}\right)^{k_l}\left(\frac{t+\Delta t}{\eta_l}\right)} . \quad (32)$$

Where: η_l and k_l are the life characteristic parameters of the equipment.

2) Environmental Disturbance Risk Indicators

China's electrical-gas coupled systems are mainly distributed in core regions such as the Beijing-Tianjin-Hebei region, the Yangtze River Delta, and the Guangdong-Hong Kong-Macao Greater Bay Area. They are significantly affected by external environments such as regional climate differences and extreme weather. Therefore, environmental disturbance indicators need to be taken as one of the important evaluation dimensions in risk assessment.

Taking extreme rainstorm weather as an example, this study establishes the model as Eqs. (33–34):

$$\lambda_{js,t}^{F} = \begin{cases} \xi_s e^{\gamma_s\left(d_{w,t} - D_{bw}\right)/D_w}, D_{bw} < d_{w,t} < \left(D_w + D_{bw}\right) \\ 0, d_{w,t} \le D_{bw} \end{cases} , \quad (33)$$

$$P_{js}^{F}\left(\Delta t\right) = 1 - e^{\int_t^{\Delta t} -\lambda_{js}^{F}(\tau) d\tau} . \quad (34)$$

Where: $\lambda_{js,t}^{F}$ is the fault occurrence rate; $d_{w,t}$ is the water accumulation height around the w equipment at time t; D_w is the flood control height near the substation; D_{bw} is the specified ground height of the cable joints in the substation; ξ_s is the attenuation coefficient; γ_s is the damping coefficient; $P_{js}^{F}\left(\Delta t\right)$ is the fault probability within the time period.

3.2 Consequences of fault power outage

The consequences of fault power outage quantify the impact of faults on the operation and power consumption of the power grid, which includes three types of indicators:

1) Voltage Limit Violation Risk

After a fault occurs in the distribution network, the voltage will fluctuate sharply, which has a great impact on the system power flow distribution, power equipment insulation and other issues. In severe cases, it may lead to equipment failure, power outage and other accidents. Therefore, the voltage limit violation risk per unit time is defined as Eqs.(35–36):

$$U_{\mathrm{LEVEL}} = \begin{cases} U_{\min} - U_i, U_i < U_{\min} \\ 0, U_{\min} < U_i < U_{\max} \\ U_i - U_{\max}, U_{\max} < U_i \end{cases} , \quad (35)$$

$$S\left(U_{\mathrm{LEVEL}}\right) = \frac{1}{T_1}\left(\frac{1}{N_z}\sum_{i=1}^{N_z} U_{\mathrm{LEVEL}}\right) . \quad (36)$$

Where: U_{LEVEL} is the voltage limit violation amount; T_1 is an evaluation period; N_z is the total number of system nodes.

2) Power Supply Interruption Load

In this study, a load weight factor is introduced to weight loads of different importance, and the load power supply interruption amount is defined as Eq. (37):

$$S_{\mathrm{loss}} = \frac{\sum_{i=1}^{\left(N_{\mathrm{loss}} - N_{DG}\right)} P_i \times \omega_i}{\sum_{i=1}^{N_{\mathrm{all}}} P_j \times \omega_j} . \quad (37)$$

Where: N_{loss} is the number of nodes downstream of the fault node; N_{DG} is the number of nodes recoverable by distributed power sources.

3) Power Outage Economic Loss

The economic loss per hour of load power outage during a fault is as Eq. (38):

$$S_m = \sum_{i=1}^{N_{loss} - N_{DG}} \pi_i \times P_i . \quad (38)$$

Where: π_i is the economic loss of a one-kilowatt load operating for one hour.

3.3 Grey relational TOPSIS method based on analytic hierarchy process (AHP) weighting

The TOPSIS method can calculate the distance between the scheme and the target. This study focuses on fault prevention, so the relative importance adopted in the weighting process is shown in Table 3.

The importance levels of the respective elements are defined as follows [29–30]:

- The operational reliability index serves as the core prerequisite metric and the fundamental basis for risk assessment, and is thus assigned the highest importance.
- The voltage violation risk index takes the second priority. Post-fault voltage violations directly jeopardize the secure operation of the power grid and may

Table 3 Table of relative importance for weighting

Relative importance degree	Value
The two elements are of equal importance	1
The first indicator is slightly more important than the second	3
The first indicator is obviously more important than the second	5
The first indicator is strongly more important than the second	7

trigger secondary faults, whose impact outweighs load loss and economic loss.

- The load loss rate is closely associated with the power supply guarantee of critical loads and directly determines power supply reliability, bearing greater importance than mere economic losses.
- The customer economic loss represents an indirect manifestation of fault consequences derived from load loss and grid damage, and therefore holds the lowest importance.

The entropy weight method is an objective evaluation technique that exploits the implicit information embedded in raw data to enhance the discriminability among indicators [31]. The detailed principle of this method is elaborated as follows:

- Judgment matrix $X_{sq,ij}$ is formulated according to the relative importance of each element. The specific entries of the normalized matrix are given as Eq. (39):

$$x'_{sq,ij} = \frac{X_{sq,ij}}{\sum_{i=1}^{m_{sq}} x_{sq,ij}} . \tag{39}$$

- The information entropy of the j-th indicator is defined as:

$$e_{sq,j} = -k_{sq} \sum_{i=1}^{m_{sq}} x_{sq,ij} \ln x_{sq,ij} . \tag{40}$$

- The entropy weight of the j-th indicator is defined as:

$$\lambda'_j = \frac{1-e_{sq,j}}{\sum_{j=1}^{n_{sq}} \left(1-e_{sq,j}\right)} . \tag{41}$$

The aforementioned entropy weight method derives weights solely from the dispersion of indicator values across evaluation samples, which endows it with mathematical objectivity and rigor. Nevertheless, it fails to incorporate domain-specific engineering experience and decision-making preferences, which tends to cause deviations between the allocated weights and the practical engineering importance of each indicator. To address this limitation, this paper develops a combined weighting scheme by integrating the analytic hierarchy process (AHP) with the entropy weight method, where subjective weights are employed to revise and complement the objective weights. [32]

The solution procedure is described as follows:

- Normalize each column of the judgment matrix.
- Sum the entries in each row of the normalized matrix and take the average value to obtain the initial weights.
- Calculate the product of the judgment matrix and the weight vector to derive the maximum eigenvalue.
- A consistency check is performed to quantify the calculation error. The result satisfies the test requirement if the consistency ratio is less than 0.1. The consistency ratio is computed as:

$$R_{CR} = \frac{R_{CI}}{R_{RI}} , \tag{42}$$

$$R_{CI} = \frac{\lambda_{\max} - n_{AHP}}{n_{AHP-1}} . \tag{43}$$

Where: R_{CR} is the consistency ratio; R_{CI} is the consistency index; R_{RI} is the average random consistency index; $\lambda_{\max}$ is the maximum eigenvalue of the judgment matrix; n_{AHP} is the order of the judgment matrix.

Obtain weights through *AHP*:

$$\lambda = \frac{V_{AHP,i}}{\sum_{i=1}^{n_{ABP}} V_{AHP,i}} . \tag{44}$$

Where: $V_{AHP,i}$ is the *i*-th element in the eigenvector corresponding to the maximum eigenvalue.

The AHP-based weighting method accounts for subjective decision preferences but lacks sufficient objectivity. By contrast, the entropy weight method allocates weights entirely based on objective data properties. Accordingly, the two methods are integrated to achieve combined weighting:

$$\lambda_j = \frac{\lambda'_j \lambda''_j}{\sum \lambda'_j \lambda''_j} . \tag{45}$$

The core principle of the TOPSIS method is to construct positive and negative ideal target solutions as evaluation benchmarks and take the distance between the evaluated scheme and the ideal solution as the core measurement to realize the comprehensive evaluation of schemes under multiple indicators. Its specific process is as Eqs. (46–47):

1. Optimal Ideal Target Solution

$$v_0^+ = \max v_{ti}\left(j\right), 1 \le i \le m_t \tag{46}$$

2. Grey Relational Coefficient

$$s_{h,ij} = \frac{\begin{array}{l}\min\limits_{i \le i \le m_t} \min\limits_{1 \le j \le n_t} \left|v_0^+\left(j\right) - v_u\left(j\right)\right| + \\ \rho \max\limits_{1 \le i \le m_t} \max\limits_{1 \le j \le n_t} \left|v_0^+\left(j\right) - v_u\left(j\right)\right|\end{array}}{\begin{array}{l}\left|v_0^+\left(j\right) - v_{ti}\left(j\right)\right| + \\ \rho \max\limits_{1 \le i \le m_t} \max\limits_{1 \le j \le n_t} \left|v_0^+\left(j\right) - v_{ti}\left(j\right)\right|\end{array}} \tag{47}$$

Where: ρ is the distinguishing coefficient, with a range of 0 to 1, and the commonly used value of 0.5 is adopted; $s_{h,ij}$ is the grey relational matrix.

3. Positive and negative ideal target solutions, s_{lx0}^+, s_{lx0}^- are defined as:

$$s_{lx0}^{+} = \max s_{h,i}(j), 1 \le i \le m_t , \tag{48}$$

$$s_{lx0}^{-} = \min s_{h,i}(j), 1 \le i \le m_t . \tag{49}$$

4. Calculate the distance between the power equipment risk index value and the positive and negative ideal target solutions:

$$d_{lx,i}^{+} = \sqrt{\sum_{j=1}^{n_t} \left(s_{lx,i}(j) - s_{lx0}^{+}(j) \right)^2} , \tag{50}$$

$$d_{lx,i}^{-} = \sqrt{\sum_{j=1}^{n_t} \left(s_{lx,i}(j) - s_{lx0}^{-}(j) \right)^2} . \tag{51}$$

5. Calculation of relative closeness degree:

$$D_{lx,i} = \frac{d_{lx,i}^{-}}{d_{lx,i}^{+} + d_{lx,i}^{-}}, i = 1, \ldots, m_t . \tag{52}$$

3.4 Error evaluation criterion

In this paper, the second-order cone relaxation technique is applied to relax the system model, and the maximum relative error is adopted as the evaluation metric to verify the accuracy of the relaxed model. The relaxation error of the distribution network is defined in Eq. (53), and that of the natural gas network is given in Eq. (54):

$$\Delta_{ij,t} = \left| i_{ij,t} - \frac{P_{ij,t}^2 + Q_{ij,t}^2}{u_{i,t}} \right| , \tag{53}$$

$$\Delta_{mn,t} = \left| \frac{W_{mn,t}^2 - C_{mn}^2 \left(G_{m,t}^2 - G_{n,t}^2 \right)}{W_{mn,t}^2} \right| . \tag{54}$$

4 Case analysis

4.1 Equipment risk assessment

In this study, the equipment at nodes 16, 24, 28, 31, and 32 is selected as the research object, with a risk cycle of 1 hour. This work employs operational data from an electricity-gas coupled system located in a typical region of southern China [30]. The following equipment operation indicators can be set:

Based on the data in Tables 4 and 5, initial matrix X_t is constructed, and its corresponding normalized matrix Z_t is derived as Eqs. (55–56):

Table 4 Operation indicators of partial equipment

Equipment location	Self-failure probability index	Environmental disturbance risk index
16	0.3	2.0
24	0.1	1.2
28	0.2	1
31	0.2	1
32	0.1	1

Table 5 Risk indicators of partial equipment

Operational reliability index	Voltage violation risk	Power interruption load	Economic loss of power outage
0.6	0.139	0	0
0.12	0.0147	0.49	1810.2
0.2	0.0182	0.207	1036.8
0.1	0.0186	0.534	1166.4
0.2	0.0184	0.0517	259.2

$$X_t = \begin{bmatrix} 0.6 & 0.139 & 0 & 0 \\ 0.12 & 0.0147 & 0.490 & 1810.2 \\ 0.2 & 0.0182 & 0.207 & 1036.8 \\ 0.1 & 0.0186 & 0.534 & 1166.4 \\ 0.2 & 0.0184 & 0.0517 & 259.2 \end{bmatrix} , \tag{55}$$

$$Z_t = \begin{bmatrix} 0.8804 & 0.9734 & 0 & 0 \\ 0.1761 & 0.1029 & 0.6486 & 0.7530 \\ 0.2935 & 0.1275 & 0.2740 & 0.4312 \\ 0.1467 & 0.1303 & 0.7068 & 0.4852 \\ 0.2935 & 0.1289 & 0.0684 & 0.1078 \end{bmatrix} . \tag{56}$$

The AHP judgment matrix is constructed and verified via consistency check, yielding a consistency ratio (CR) of 0.0303, which is below the threshold of 0.1 and thus satisfies the consistency requirement.

The weights derived from the AHP method are calculated according to the corresponding formulas as Eq. (57):

$$\lambda'' = \begin{bmatrix} 0.572 & 0.285 & 0.118 & 0.025 \end{bmatrix}^T . \tag{57}$$

The weights derived from the entropy weight method are as Eq. (58):

$$\lambda' = \begin{bmatrix} 0.1488 & 0.3236 & 0.2878 & 0.2397 \end{bmatrix}^T . \tag{58}$$

The weights obtained by the coupled weighting method are as Eq. (59):

$$\lambda_j = \begin{bmatrix} 0.3917 & 0.4244 & 0.1563 & 0.0276 \end{bmatrix}^T . \tag{59}$$

The weighted normalized matrix is constructed as Eq. (60):

$$V_t = \begin{pmatrix} 0.3449 & 0.4115 & 0.0000 & 0.0000 \\ 0.0690 & 0.0435 & 0.1013 & 0.0208 \\ 0.1150 & 0.0539 & 0.0428 & 0.0119 \\ 0.0575 & 0.0551 & 0.1105 & 0.0134 \\ 0.1150 & 0.0545 & 0.0107 & 0.0030 \end{pmatrix} . \tag{60}$$

The sets of the best and worst ideal target solutions are determined as Eqs. (61–62):

$$v_0^+ = [0.3449, 0.4115, 0.1105, 0.0208], \tag{61}$$

$$v_0^- = [0.0575, 0.0435, 0.0000, 0.0000]. \tag{62}$$

The grey relational matrix is obtained as Eq. (63):

$$S_h = \begin{pmatrix} 1.0000 & 1.0000 & 0.6249 & 0.8986 \\ 0.4000 & 0.3333 & 0.9529 & 1.0000 \\ 0.4445 & 0.3397 & 0.7312 & 0.9540 \\ 0.3903 & 0.3405 & 1.0000 & 0.9614 \\ 0.4445 & 0.3401 & 0.6484 & 0.9118 \end{pmatrix}. \tag{63}$$

The maximum and minimum values are extracted from each column of the grey relational matrix to serve as the grey ideal solutions:

$$s_{lx0}^+ = [1.0000, 1.0000, 1.0000, 1.0000], \tag{64}$$

$$s_{lx0}^- = [0.3903, 0.3333, 0.6249, 0.8986]. \tag{65}$$

The relative closeness degree of the risk indicators for each piece of power equipment is calculated as Eq. (66):

$$D_{lx,i} = [0.6992 \quad 0.2766 \quad 0.1271 \quad 0.2973 \quad 0.0611]. \tag{66}$$

The final risk ranking obtained by the coupled weighting method is: Device 1 > Device 4 > Device 2 > Device 3 > Device 5

Similarly, the relative closeness degrees of the risk indicators for power equipment derived from the entropy weight method are as Eq. (67):

$$D_{lx,i}{}' = [0.4941 \quad 0.4818 \quad 0.2038 \quad 0.4299 \quad 0.0614]. \tag{67}$$

The final risk ranking yielded by the entropy weight method is: Device 1 > Device 2 > Device 4 > Device 3 > Device 5

It should be noted that the above comparative analysis is conducted only for the test system and specified fault scenarios in this paper to verify the rationality and applicability of the coupled weighting method under such scenarios and does not constitute a universal proof of the method's ranking accuracy.

4.2 Reconfiguration strategy

The hardware platform for implementing the proposed method is a laptop equipped with an Intel(R) Core (TM) i7-8505U CPU and 16 GB of RAM. The simulation is performed in the MATLAB R2024a environment. The mixed-integer second-order cone programming (MISOCP) model is constructed and solved by calling the CPLEX solver via the YALMIP toolbox.

To focus on the core verification of the fault recovery coordination mechanism and SOP regulation characteristics, the model proposed in this paper is established based on the following premises and assumptions:

- The system is assumed to be equipped with reliable full-domain communication links, and the operational state data of both the distribution network and natural gas network can be acquired completely and accurately. Issues such as communication interruption, data loss and transmission delay under extreme disaster scenarios are not considered in the current work.
- The optimization calculation of the model is carried out with deterministic time-series forecast values of electric load, natural gas load and renewable energy generation, and the input forecast data are assumed to satisfy the accuracy requirement for engineering applications by default.
- This study focuses on recovery optimization under deterministic fault scenarios, and the stochastic propagation characteristics of uncertain factors, including random fluctuations in renewable energy output and dynamic disturbances of natural gas load, have not been systematically incorporated.

To prevent the evolution of a single fault into a systematic fault, this study adopts the coordinated operation of energy storage devices and SOP at node 7 and node 13 to restore power-loss loads. This improves the power supply flexibility of the system, reduces natural gas demand, and regulates the output of gas-fired units. It ensures that the gas network will not experience parameter violation or trigger the protection mechanism of gas-fired units due to excessive power load demand, thereby effectively avoiding the off-grid of gas-fired units.

To further explore the precise regulation effect of SOP in the fault recovery of integrated electricity-gas coupled systems, two differentiated control strategies are established for simulation analysis. The first is the optimal control strategy of SOP coordinating with gas-fired unit output. By virtue of the precise power flow regulation capability of SOP, it avoids the off-grid accident of gas-fired units caused by power limit violation and guarantees the stable operation of the electricity-gas coupled system. The second is the strategy without SOP participating in the output regulation of gas-fired units, which only relies on traditional section switches to complete fault isolation and network reconfiguration.

The fault test scenarios in this simulation are established based on the actual evolution pattern of cascading failures under rainstorm disasters in the study area. The initially failed facilities focus on rainstorm-high-risk components including overhead distribution lines, outdoor switch stations and gas pressure regulating stations. A contingency set is built according to the risk assessment grades of the five aforementioned devices:

- Contingency 1: The equipment at node 16 and node 31 fails, and the corresponding lines are disconnected;
- Contingency 2: Devices at nodes 16, 31, 24 and 28 suffer failures, and the corresponding lines are disconnected;
- Fig. 3 shows the comparison curve between renewable energy output and active power consumption of loads.

4.3 Fault recovery

Fig. 4 presents the fault reconfiguration diagram under Contingency 1. In the islanding scheme, traditional sectionalizing switches and SOP are respectively adopted to participate in the reconfiguration strategy. Table 6 and Table 7 list the load recovery level of the power grid and the output of gas-fired units under the two reconfiguration strategies. Fig. 5 and Fig. 6 show the system voltage curves obtained by the two reconfiguration strategies.

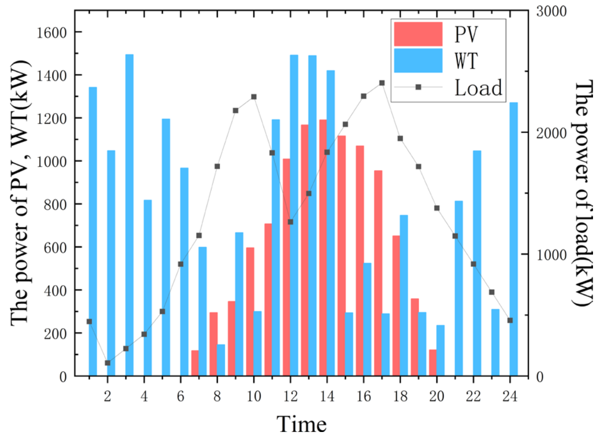

Fig. 3 Comparison of active power between energy output and load consumption

In terms of voltage distribution characteristics, affected by topology switching and power flow transfer, the traditional network reconfiguration scheme suffers from large voltage deviations in partial sections. The minimum node voltage across the network is approximately 0.977p.u., and the maximum deviation of node voltage relative to the rated value reaches about 4.9%. The highest node voltage is close to the conventional upper limit of voltage deviation for distribution networks, resulting in insufficient voltage safety margin.

With the introduction of SOP for coordinated regulation, SOP can flexibly adjust power flow distribution through active power transfer and reactive power compensation at both terminals, delivering a notable optimization of the overall voltage profile. Specifically, the minimum node voltage rises to approximately 0.987p.u., and the maximum voltage deviation drops to about 1.5%. All node voltages are maintained at levels closer to the rated value with adequate voltage safety margin. The above quantitative results verify that SOP can effectively smooth out node voltage fluctuations after fault recovery, narrow the voltage deviation range of the whole network, and improve power supply quality during the fault recovery phase.

According to the node pressure safety criteria stated in the Fluxys safety report, this study defines 85% of the maximum

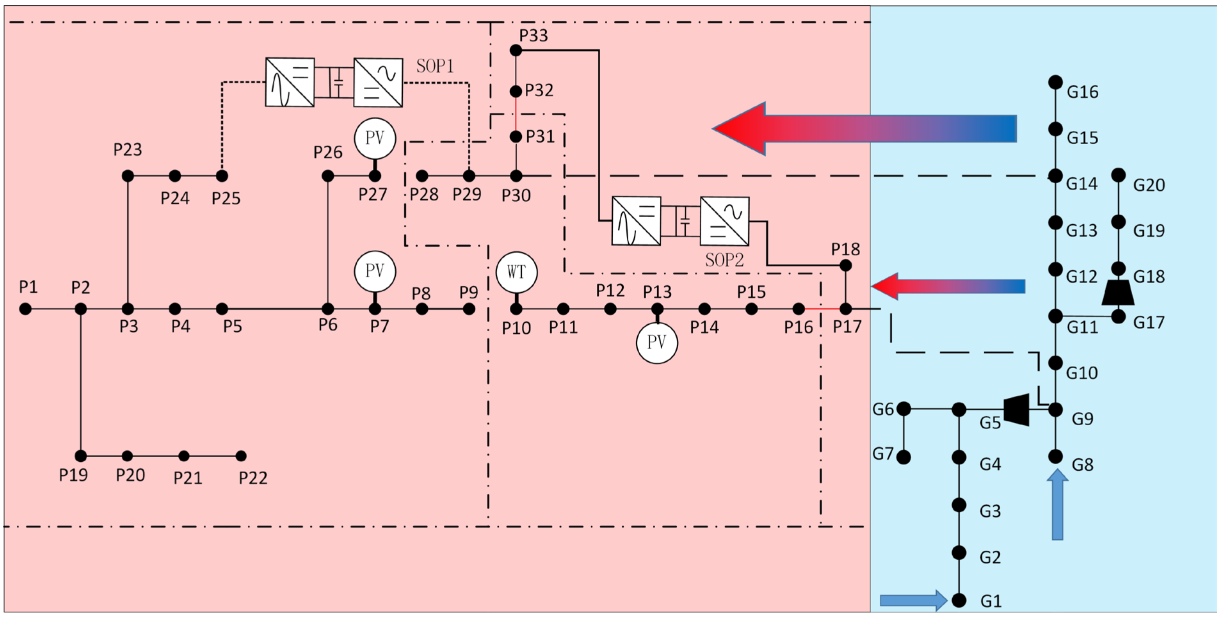

Fig. 4 Fault restoration and reconfiguration diagram for contingency 1

Table 6 Results under traditional reconfiguration

Output Increment/MW	Power-loss Nodes	Curtailed Load Power/kW
1(P7), 6(P13) 3(P17), 3(P30)	14, 16, 32, 33	321

Table 7 Results of SOP-assisted reconfiguration

Output Increment/MW	Power-loss Nodes	Curtailed Load Power/kW
−1.677(P17), 1.067(P30)	/	0

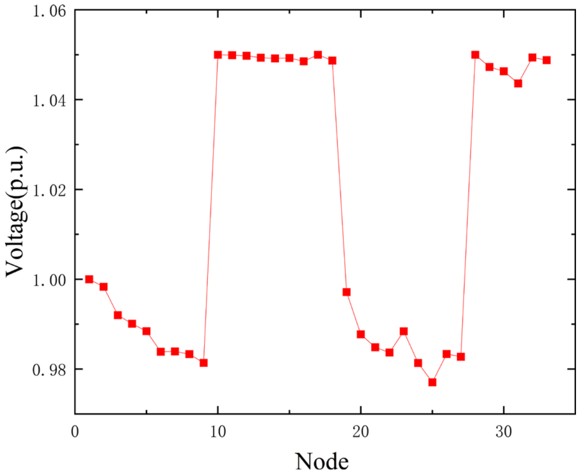

Fig. 5 System voltage under conventional reconfiguration

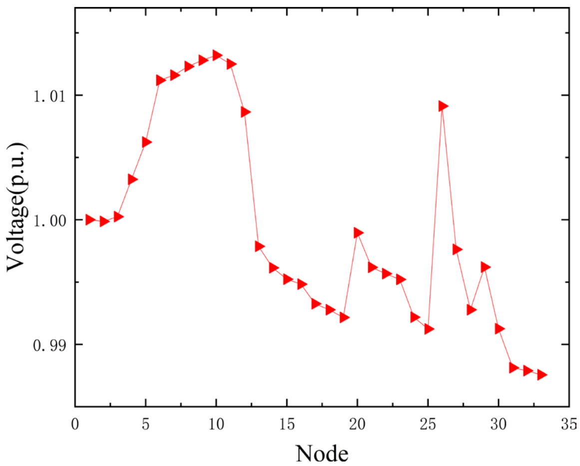

Fig. 6 System reconfiguration voltage with SOP participation

allowable node pressure limit as the first-level early warning threshold and 95% as the second-level early warning threshold. In accordance with the Chinese Code for Design of City Gas Engineering (GB 50028-2006, 2020 Edition), the operating pressure of gas pipelines shall not exceed the design pressure (i.e., MAOP). In engineering practice, a safety margin of 10%–15% is generally reserved to avoid overpressure risks caused by transient pressure shocks from load fluctuations and scheduling adjustments. The two-level thresholds adopted in this paper are highly consistent with industrial engineering conventions:

- The threshold of 85% MAOP serves as the pre-warning criterion, reserving a 15% buffer margin below the maximum pressure limit to activate preventive regulation, which corresponds to the conventional alert level for daily safety management;
- The threshold of 95% MAOP acts as the extreme constraint criterion with only a 5% limit margin, representing the overpressure red line under fault conditions. Once this threshold is reached, emergency control measures are triggered to guarantee the operational safety of gas pipelines and prevent overpressure failure.

Once the node pressure reaches the second-level early warning threshold, immediate pressure reduction measures shall be adopted to prevent operational risks of the natural gas network.

From the operation results of the traditional switch reconfiguration scheme, limited by the topological adjustment capability of conventional sectionalizing switches, it is impossible to restore all loads after the fault. Consequently, power loss occurs at nodes 14, 16, 32 and 33, with the curtailed load power reaching 321kW, which significantly impairs the power supply reliability. Meanwhile, to compensate for the power shortage, multiple gas-fired units in the system are forced to increase output substantially; Units P17 and P30 each increase their output by 3MW. The drastic output adjustment of the units directly causes severe pressure fluctuation at gas network nodes. As shown in Fig. 7, under the conventional reconfiguration mode, the gas pressure at nodes 8 and 9 exceeds the second-level early warning threshold, while the pressure at nodes 1, 3, 5, 10, 11 and

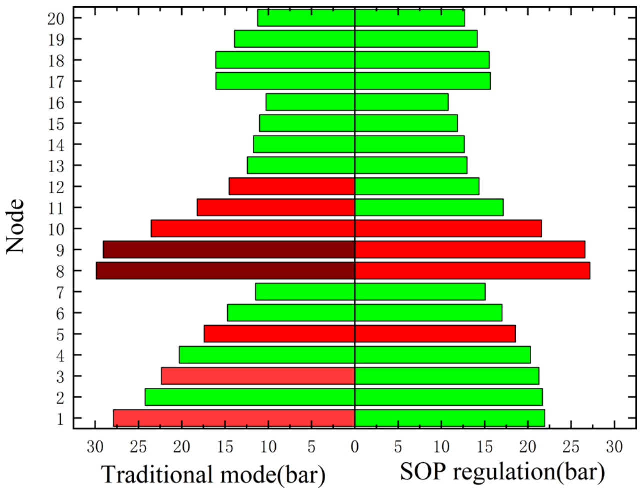

Fig. 7 Comparison of gas network pressure under different strategies

12 enters the first-level early warning range. The operating parameters of the gas network approach the safety boundary, the system safety margin is greatly reduced, and obvious operational risks exist.

In contrast, the collaborative reconfiguration scheme with SOP participation presents prominent performance advantages. Through collaborative topology optimization of SOP and sectionalizing switches, the system successfully realizes full restoration of all loads after the fault, the curtailed load power is reduced to 0kW, and the power supply reliability is fully guaranteed. With the precise power flow regulation of SOP, only minor output adjustments are required for gas-fired units. Specifically, the output of Unit P17 decreases by 1.6777MW, and the output of Unit P30 increases by 1.067MW, with the output variation far lower than that of the traditional scheme. In terms of gas network operating conditions, after SOP participates in reconfiguration, the gas pressure of all nodes remains steadily within the first-level early warning range, and no node enters the second-level early warning interval, completely eliminating the potential safety hazards of the gas network under the traditional scheme.

It is evident that the collaborative reconfiguration strategy involving SOP not only solves the problem of insufficient load restoration in the traditional scheme, but also avoids drastic output adjustments of gas-fired units via precise power flow regulation. It effectively suppresses the pressure fluctuation of gas network nodes and blocks the fault propagation of the integrated electricity-gas coupled system. Table 8 presents the comparison of gas pressure safety margins under the conventional reconfiguration method and the SOP-based reconfiguration method.

Considering that the failure mechanism, system response characteristics and restoration objectives of Contingency 2 are basically consistent with those of Contingency 1, repeated case analysis and result elaboration for Contingency 2 are omitted in this paper. The simulation results verify that under the scenario of Contingency 2, the SOP-coordinated reconfiguration strategy and hierarchical maintenance schedule can still achieve full load restoration, stable gas network pressure and improved system resilience.

For the benchmark scenario of the IEEE 33-node distribution network coupled with a 20-node natural gas system, the proposed MISOCP restoration model achieves an average solution time of approximately 2-3s per scenario. This duration is far below the 30-second general engineering threshold for online fault restoration decision-making in distribution networks and can fully satisfy the timeliness requirement of offline scheduling decisions after fault occurrence.

Traditional network reconfiguration relies on the mechanical operations of sectionalizing switches and tie switches. A single switching operation typically takes several seconds to tens of seconds, and the entire reconfiguration process with coordinated multi-switch operations may take up to minutes. By contrast, as a fully controllable power electronic device, the soft open point (SOP) involves no mechanical action. Its command response time for active and reactive power regulation ranges from 10ms to 50ms, and the steady-state transition process lasts no more than 200ms. By combining the algorithm computation time and the SOP power regulation time, the full-cycle response from scheme generation to regulation implementation can be controlled within several seconds. This enables rapid power flow redistribution and voltage support immediately after fault isolation, effectively shortens the duration of voltage sags, and improves power supply quality during the restoration phase.

In this paper, the nonlinear gas flow constraints of the natural gas network are converted into convex constraints via second-order cone relaxation, and the overall model is formulated as a standard MISOCP problem with polynomial-time solvability. The computational complexity grows at a controllable rate with the expansion of system nodes and equipment scale. Supported by the branch-and-bound and cutting-plane optimization algorithms embedded in mature commercial solvers, the proposed method possesses theoretical scalability for medium- and large-scale regional integrated electricity-gas systems.

4.4 Maintenance schedule

After distribution network line failures caused by extreme weather, the system first completes accurate location of fault areas and island division based on the equipment

Table 8 The comparison of gas pressure safety margins

Node	1	2	3	4	5	6	7	8	9	10	11	12	13	14	15	16	17	18	19	20
The conventional reconfiguration method/%	7	19	10	18	12	26	42	0.4	3	5	8	3	17	21	26	31	19	19	30	43
The SOP-based reconfiguration method/%	26	27	14	18	7	14	24	9	11	13	14	4	13	15	20	28	21	22	29	36

fault risk assessment results. Through the coordinated regulation of SOP, sectionalizing switches and power output devices, rapid isolation of fault sections and power supply restoration of non-fault sections are realized.

In the fault disposal and maintenance process, the principle of priority maintenance for high-risk equipment is strictly followed. Critical equipment with higher rankings in risk assessment is repaired preferentially to minimize the impact of faults on the safe and stable operation of the integrated electricity-gas coupled system. In this paper, the maintenance cycle of a single fault is set to 6 hours. After the faulty equipment is overhauled and potential safety hazards in the fault section are eliminated, the system initiates the grid-reconnection restoration process and gradually returns to the normal power supply state.

Relying on the bidirectional power flow regulation capability of SOP, the system coordinates coupled units such as gas turbines to optimize power distribution, greatly improves the local consumption rate of distributed renewable energy, and achieves comprehensive enhancements in power supply reliability, energy utilization efficiency and system economic performance during fault restoration. This study adopts Contingency 2 induced by extreme weather events to evaluate the performance of the two different weighting methods. The detailed verification procedure is implemented as follows:

After the fault occurs, the first-stage maintenance plan is carried out, with a maximum of 2 fault points repaired in each maintenance stage. Fig. 8 presents the maximum tolerable gas pressure for natural gas network nodes. Fig. 9 illustrates the line current-carrying capacity of the distribution network after the first-stage maintenance.

Fig. 10 presents the schematic of switching actions for different maintenance paths derived from the entropy weight method and the coupled weighting method, along with a comparison of fault maintenance sequences between the two methods.

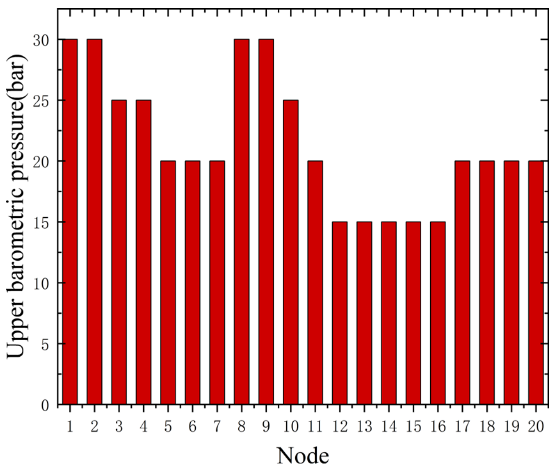

Fig. 8 Upper limit of node gas pressure

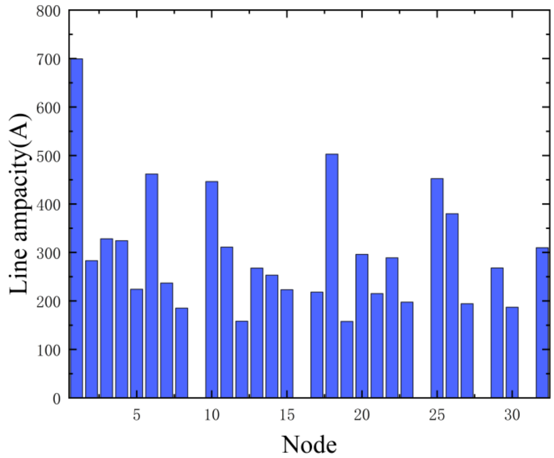

Fig. 9 System current-carrying capacity after the first reconfiguration

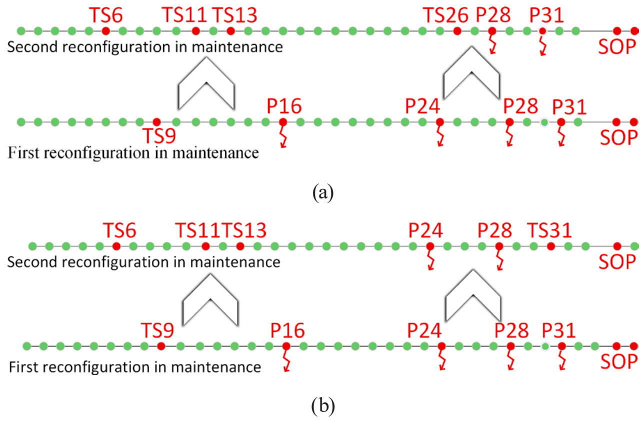

Fig. 10 Schematic of switching actions under two sequencing methods and system current-carrying capacity after the first reconfiguration: (a) Entropy weight-based sequencing method; (b) Coupled weighting-based sequencing method

This study adopts 700A as the upper limit of current-carrying capacity for the 10kV distribution network in accordance with engineering standards.

Fig. 11 presents the current-carrying capacity of the distribution network system upon completion of the first-stage maintenance (i.e., the second reconfiguration).

Key observations from Fig. 11 are summarized as follows:

- The current-carrying capacity distribution under the coupled weighting method exhibits lower peak values. At high-load nodes 18 and 25, the current-carrying capacities yielded by the entropy weight-based sequencing method are 592.4A and 536.44A, respectively, whereas those obtained by the coupled weighting-based sequencing method reach 230A and 212.62A. It is evident that the coupled weighting method outperforms the entropy weight method in smoothing the current amplitude.

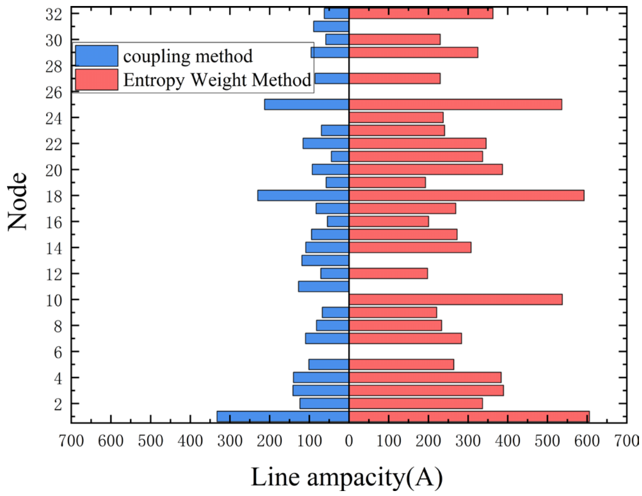

Fig. 11 Schematic of switching actions under two different sequencing methods

- When addressing faults at Nodes 16 and 24, the entropy weight method achieves optimality in terms of specific local indicators, but may trigger secondary overloads across the global network. Under the maintenance sequence of the entropy weight method, the current-carrying capacity of several nodes remains at a high level, which elevates the risk of secondary line failures induced by overheating in actual system operation.
- Benefiting from the integration of subjective empirical weights, the coupled weighting method embeds pre-assessment of power grid safety limits into maintenance decision-making. This allows the maintenance sequence to proactively circumvent vulnerable lines that are susceptible to cascading failures during implementation.
- As shown in Table 9, there is no remarkable difference in energy storage output between the two sequencing methods. Specifically, the energy storage output derived from the coupled weighting method is even 1.478kW lower than that of the entropy weight method.

Accordingly, for complex reconfiguration tasks involving multi-point consecutive faults, the coupled weighting method that combines subjective and objective weights possesses a decision logic more aligned with the fundamental demands of power system security defense and high-reliability power supply.

Table 9 Energy storage output under the two different sequencing methods

Entropy weight method		Coupled weighting method	
Node13/kW	Node27/kW	Node13/kW	Node27/kW
1.238	−1.977	1.193	−1.912

The rolling adjustment mechanism and operating margin analysis proposed in this study only address the time-sequential dynamic scheduling requirements during the fault recovery process, and are intended to accommodate the fault evolution process and time-sequential load fluctuations. They do not constitute a comprehensive uncertainty analysis that accounts for stochastic factors such as random fluctuations of source and load and equipment failure probabilities.

5 Error analysis

Fig. 12 presents the relaxation gap of the distribution network calculated via Eq. (53), which can be narrowed down to the order of 10-4kA. This verifies that the error introduced by the second-order cone relaxation can satisfy the system operational requirements.

Fig. 13 presents the pipeline gas flow error results of the gas distribution network. The relaxation achieves favorable performance on the vast majority of pipelines, which fully validates its effectiveness as an efficient solution

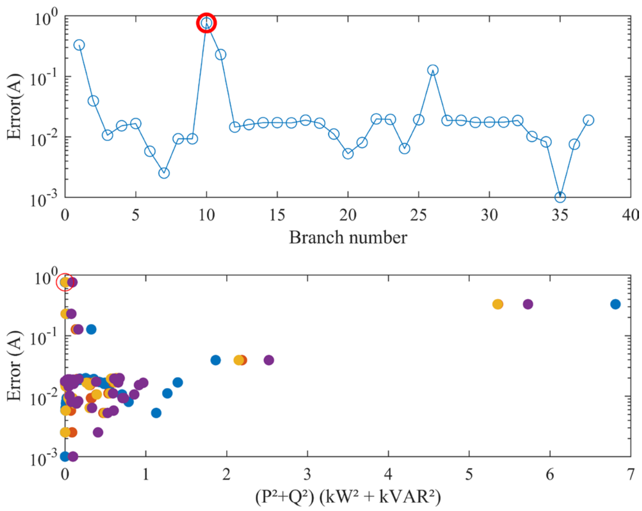

Fig. 12 Error profile of the distribution network

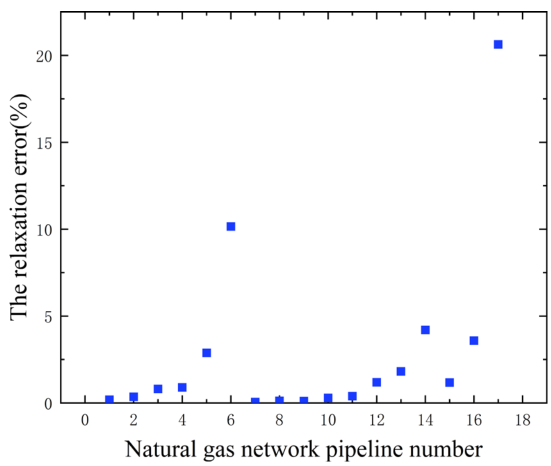

Fig. 13 Error profile of the natural gas network

approach for large-scale gas network optimization problems. However, two pipelines in the figure exhibit remarkably higher errors. This observation is fully consistent with the widely reported limitations of such relaxation methods in the literature, and it stems from the inherent strong nonlinearity of the Weymouth equation, which degrades the approximation accuracy of the relaxation. [33]

Despite these local errors, given that they only account for 10% of the total pipelines and mainly affect the accuracy of local flow estimation, the solutions derived from the relaxation method still maintain sufficient accuracy and feasibility at the system level when solving global optimization problems.

6 Conclusion

To address the frequent cascading failures, severe load outage during maintenance, and insufficient resilience of electricity-gas coupled systems under extreme weather, this paper establishes an equipment risk assessment model based on risk early warning and proposes a fault reconfiguration and hierarchical maintenance restoration strategy with coordinated SOP and energy storage. For risk assessment, a subjective-objective coupled weighting method integrating entropy weight and AHP is adopted to optimize the decision-making of equipment maintenance priority.

Simulation results verify that the proposed method can effectively block the propagation paths of cross-domain cascading failures and achieve full post-fault load restoration as well as safe and stable operation of the gas network. Compared with the single entropy weight method, the maintenance sequence derived from coupled weighting yields lower peak current-carrying capacity, avoids the risk of secondary overload induced by local optimum, and proactively circumvents vulnerable lines. Its decision logic aligns better with the requirements of power system security defense and further improves the resilience of the coupled system.

This study breaks through the limitations of traditional single-system restoration. Nevertheless, the coupled weighting framework is only verified based on a single system and typical scenarios, with limited verification dimensions. In follow-up research, the set of fault working conditions can be expanded, or Monte Carlo simulation can be adopted to extend the analysis to multiple scenarios and compare various classical decision-making methods, so as to verify the universality and robustness of the proposed method.

Acknowledgement

This work was supported by National Fund Project (No. 52567011); Central Guidance For Local Development Funding Projects (No. 25ZYJA014); Gansu Province Major Science and Technology Projects (No. 22ZD6GA063); Dunhuang Technology Support Project (No. 200501, No. 200502).

References

[1] Chen, X., Huang, Y., Chen, F., Shao, Z., Huang, T. "台风灾害下计及故障演化的电-气综合能源系统分布式恢复策略"(Distributed Recovery Strategy for Integrated Electricity and Gas System Considering Failure Evolution Under Typhoon), High Voltage Engineering, 52(4), pp. 1696–1711, 2026. (in Chinese) https://doi.org/10.13336/j.1003-6520.hve.20251046

[2] Fang, Y. "英国"8 • 9"停电事故对频率稳定控制技术的启示" (Reflections on frequency stability control technology based on the blackout event of 9 August 2019 in UK), Automation of Electric Power Systems, 43(24), pp. 1–5, 2019. (in Chinese) https://doi.org/10.7500/AEPS20191011006

[3] Hou, Y., Ding, Y., Bao, M., Liang, Z., Song, Y., Guo, C. "电-气耦合视角下德州大停电事故分析及对我国新型电力系统发展启示" (Analysis of Texas blackout from the perspective of electricity-gas coupling and its enlightenment to the development of China's new power system), Proceedings of the Chinese Society of Electrical Engineering, 42(21), pp. 7764–7774, 2022. https://doi.org/10.13334/j.0258-8013.pcsee.212202

[4] Yan, D., Wen, J., Du, Z., Yang, D., Yao, W., Zhao, H., Liu, J. "2021年得州大停电事故分析及其对电网规划管理的启示" (Analysis of Texas blackout in 2021 and its enlightenment to power system planning management), Power System Protection and Control, 49(9), pp. 121–128, 2021. (in Chinese) https://doi.org/10.19783/j.cnki.pspc.210358

[5] Hong, S., Wang, H., Wu, Z., and Sheng, K. "高过流能力电力电子器件关键技术展望" (Outlook on key technologies for high overcurrent capability power electronic devices), Scientia Sinica Technologica, 56(1), pp. 79–96, 2026. (in Chinese) https://doi.org/10.1360/SST-2025-0161

[6] Jiang, Y., Li, Z., Zhu, Y., Ye, S. "A variable-weight coupling coordination degree method for evaluating the development level in meshed distribution networks considering source-load balance", Results in Engineering, 30, 110312, 2026. https://doi.org/10.1016/j.rineng.2026.110312

[7] Chen, W., Din, X., Shi, Y., Guo, C. "考虑双向耦合的电-气综合能源系统时序故障恢复方法" (Sequential fault restoration method for electricity-gas integrated energy system considering two-way coupling), Electric Power Automation Equipment, 39(8), pp. 86–94, 2019. (in Chinese) https://doi.org/10.16081/j.epae.201908006

[8] Wang, Y., Liu, C., Zhao, Y., Li, X., Wu, Y. "Load restoration strategy for post-disaster distribution networks considering cyber-physical-traffic coupling with multi-resource collaboration", Applied Energy, 407, 127373, 2026. https://doi.org/10.1016/j.apenergy.2026.127373

[9] Jia, C., Huang, B., Chuai, Z., Yan, C., Wang, Q., Li, H., Zhang, S., Chen, X. "A distributed optimization method for urban active distribution networks considering SOPs and user side flexible resources based on ADMM", Systems Science & Control Engineering, 12(1), 2394430 2024. https://doi.org/10.1080/21642583.2024.2394430

[10] Nacef, S., Babouri, R., Ghedamsi, K., Houari, A. "Fault-resilient Control Strategy for Cascaded Multilevel Inverters in Grid-connected PV Systems", Periodica Polytechnica Electrical Engineering and Computer Science, 69(2), pp. 148–158, 2025. http://doi.org/10.3311/PPee.39480

[11] Al-Dwa, A. A. M., Chebabhi, A., Defdaf, M., Guessabi, A. "New Modeling and Improved Current Control Strategy to Eliminate the Impact of Synchronization Method and Parks Transformation for Grid-connected Four-leg PWM Inverter", Periodica Polytechnica Electrical Engineering and Computer Science, 67(2), pp. 204–215, 2023. https://doi.org/10.3311/PPee.20517

[12] Kang, Y., Lu, G., Chen, M., Li, X., Li, S. "Fault recovery method of DC distribution network considering EV charging and discharging and SOP network reconfiguration", Electric Power Systems Research, 245, 111607, 2025. https://doi.org/10.1016/j.epsr.2025.111607

[13] Hu, Z., Yang, X., Ding, L., Li, Z., He, Y., Wu, Q., Wen, J. "Measurement-Correlated Resilience Enhancement for R-SOP-Integrated Distribution Systems With Voltage Security", IEEE Transactions on Smart Grid, 16(6), pp. 4517–4533, 2025. https://doi.org/10.1109/TSG.2025.3594669

[14] He, X., Gao, H., Wang, R., Luo, L., Ye, M., Huang, Y., Liu, J. "基于图深度强化学习的有源配电网故障恢复方法" (Fault Recovery Method for Active Distribution Networks Based on Graph Deep Reinforcement Learning), Power System Technology, 49(10), pp. 4342–4352, 2025. (in Chinese) https://doi.org/10.13335/j.1000-3673.pst.2024.2215

[15] Peng, H., Zhang, L., Tan, M., Su, Y., Li, H. "重构与抢修协同下电 – 气区域综合能源系统多阶段博弈故障恢复方法" (Multi-Stage Game Fault Recovery Method for Regional Electricity-Gas Integrated Energy System Under Collaborative Reconfiguration and Rush Repair), Electric Power Construction, 45(12), pp. 27–38, 2024. (in Chinese) http://doi.org/10.12204/j.issn.1000−7229.2024.12.003

[16] Zhang, R., Yang, Z., Yan, K. "区域电-气综合能源系统故障恢复与维修协调优化策略" (Coordinated Optimization Strategy for Fault Recovery and Maintenance of Regional Electricity-Gas Integrated Energy System), Journal of Northeast Electric Power University, 43(4), pp. 90–100, 2023. (in Chinese) https://doi.org/10.19718/j.issn.1005-2992.2023-04-0090-11

[17] Zhang, G. "考虑分布式电源接入的配电网 – 天然气互联系统可靠性评估" (Reliability Assessment of Distribution Network-Natural Gas Interconnection System Considering Distributed Generation Integration), Dissertation Shandong University, 2025. (in Chinese) https://doi.org/10.27272/d.cnki.gshdu.2025.001959

[18] Ye, Z., Zhang, X., Wu, J., Luo, X. "无人平台综合电力系统连锁故障风险评估模型及预防策略" (Risk Assessment Model and Prevention Strategy for Cascading Failures of Integrated Power System on Unmanned Platforms), Acta Armamentarii, 46(S1), pp. 236–249, 2025. (in Chinese) https://doi.org/10.12382/bgxb.2025.0514

[19] Zhang, A., Li, J., Lin, D., Yang, W., Li, Q., Qu, G. "考虑天然气管网极限风险影响的电-气耦合系统连锁故障模型" (Cascading Failure Model of Electricity-Gas Coupled System Considering the Impact of Natural Gas Pipeline Network Limit Risk), Proceedings of the CSEE, 41(21), pp. 7275–7285, 2021. (in Chinese) https://doi.org/10.13334/j.0258-8013.pcsee.201959

[20] Wang, K., Xue, Y., Zhou, Y., Li, Z., Chang, X., Sun, H. "Distributed coordinated reconfiguration with soft open points for resilience-oriented restoration in integrated electric and heating systems," Applied Energy, 365, 123207, 2024. https://doi.org/10.1016/j.apenergy.2024.123207

[21] Yang, K., Zhao, Z., Zhang, A., Yang, W., Li, Q., Zeng, S., Peng, G. "Risk modelling of hydrogen-enriched natural gas on pipelines and gas-electric coupled systems", IET Energy Systems Integration, 6(3), pp. 253–267, 2024. https://doi.org/10.1049/esi2.12124

[22] Yan, Y., Yan, J., Liu, S., Wang, Y., Wang, B., Han, S., Yongqian, L. "Review and prospect on the construction method of security region for integrated natural gas and power systems", Energy, 307, 132543, 2024. https://doi.org/10.1016/j.energy.2024.132543

[23] Bahlouli, H., Mansouri, A., and Bouhamida, M. "Comparative study of robust RSC control of doubly fed induction generator based wind turbine under grid frequency and voltage variations", Periodica Polytechnica Electrical Engineering and Computer Science, 67(4), pp. 449–457, 2023. https://doi.org/10.3311/PPee.21333

[24] Wang, W., Xie, K., Wang, H., Chen, T., Chen, H., He, Y. "Coordinating O&M and logistical resources to enhance post-disaster resilience of interdependent power and natural gas distribution systems", Reliability Engineering & System Safety, 267, 111875, 2026. https://doi.org/10.1016/j.ress.2025.111875

[25] Li, Z., Zhang, T., Xu, B., Zhao, X., Ye, Y., Fu, Y. "计及运行风险的配电网故障后供电恢复决策及广义动态孤岛划分" (Post-Fault Power Supply Recovery Decision and Generalized Dynamic Island Partition of Distribution Network Considering Operation Risk), Modern Electric Power, 42(2), pp. 281–292, 2025. (in Chinese) https://doi.org/10.19725/j.cnki.1007-2322.2023.0022

[26] Ye, Y., Zhou, F., Zhang, B., Hu Z., Yang, X. "协调故障重构和智能软开关的柔性配电系统故障恢复策略" (Fault Recovery Strategy for Flexible Distribution System Coordinating Fault Reconfiguration and Soft Open Point), Proceedings of the CSU-EPSA, 37(01), pp. 74–83, 2025. (in Chinese) https://doi.org/10.19635/j.cnki.csu-epsa.001468

[27] Jia, W., Ding, T., Qu, M., Bai, J., He, Y., Cheng, T. "适用能源互联网非线性气流方程组的线性优化求解模型" (Linear Optimization Solution Model for Nonlinear Gas Flow Equations in Energy Internet), Proceedings of the CSEE, 40(24), pp. 7938–7949+8231, 2020. (in Chinese)
https://doi.org/10.13334/j.0258-8013.pcsee.191650

[28] Chen, H., Gao, K., Zhang, R., Jiang, T., Yan, K., "考虑异步通信的配电 – 气网分布式有功 – 无功协同优化" (Distributed Active-Reactive Power Coordinated Optimization of Distribution-Gas Network Considering Asynchronous Communication), Automation of Electric Power Systems, 48(20), pp. 69–80, 2024. (in Chinese)
https://doi.org/10.7500/AEPS20240330006

[29] Zhu, J., Luo, T., Wu, W. Li, S., Dong, H. "综合能源系统运行可靠性评估评述 Ⅰ：模型驱动法" (Review on Operational Reliability Assessment of Integrated Energy System Part I: Model-Driven Method), Transactions of China Electrotechnical Society, 37(11), pp. 2761–2776, 2022. (in Chinese)
https://doi.org/10.19595/j.cnki.1000-6753.tces.210927

[30] Liang, Z., Kang, C., Sui, L., Yu, R., Jia, Y., Du, Y., Cheng, W. "含高比例分布式光伏的主配网运行风险评估与防控策略研究" (Research on Operational Risk Assessment and Prevention-Control Strategy of Transmission and Distribution Network with High Proportion of Distributed Photovoltaics), Journal of Tsinghua University (Science and Technology), 64(11), pp. 1964–1978, 2024. (in Chinese)
https://doi.org/10.16511/j.cnki.qhdxxb.2024.27.011

[31] Tan, J., Wang, K., Yu, B., Nan, D., Liu, H. "基于熵权法的电力二次设备健康状态评估" (Health Status Assessment of Power Secondary Equipment Based on Entropy Weight Method), Journal of Shenyang University of Technology, 47(4), pp. 425–431, 2025. (in Chinese)
https://doi.org/10.7688/j.issn.1000-1646.2025.04.03

[32] Zhang, M., Yang, X., Guan, C., Yang, P., Deng, R., Wang, Y. "Research on the comprehensive performance evaluation framework of hybrid energy storage system for all-electric ships based on AHP and entropy weight method", In: Proceedings of the 7th IEEE International Conference on Transportation Information and Safety (ICTIS 2023), Xi'an, China, 2023, pp. 1021–1028. ISBN 979-8-3503-0854-9
https://doi.org/10.1109/ICTIS60134.2023.10243974

[33] Liu, T., Zhang, Q., He, C. "考虑气电联合需求响应的气电综合能源配网系统协调优化运行" (Coordinated Optimal Operation of Gas-Electricity Integrated Energy Distribution Network Considering Combined Gas-Electricity Demand Response), Proceedings of the CSEE, 41(05), pp. 1664–1677, 2021. (in Chinese)
https://doi.org/10.13334/j.0258-8013.pcsee.200385